

Order reprints and pay color figure charges online at www.sheridan.com/aaas/eoc

Dear Author:

Science has a combined online form for ordering reprints and paying charges on color figures. Please follow the link mentioned above to pay for or receive an invoice for your color figure charges. To start your order, you'll need to enter the entire DOI number of your paper (for example: 10.1126/science.1194732). After filling out the order form, an email will be sent for your records. An invoice will be sent with the reprints. You can pay at the time of your order, indicate that you have a purchase order, or ask to be billed.

Reimbursement for Use of Color in Science

As stated in Information for Contributors and your acceptance letter, authors requesting the use of color are required to pay \$650 for the first color figure and \$450 for each additional figure to help defray costs related to publishing color in the *Science* issue. **These charges are not related to your reprint order**, but are billed on the same form. Authors of solicited Reviews, Special Issue Perspectives, and Special Issue Reviews are exempt from these charges.

Printed Reprints

Author reprints must be used solely for the author's personal use. If commercial or for-profit use is intended, please contact Rockwater, Inc. at brocheleau@rockwaterinc.com or (803) 429-4933.

Only one invoice will be issued for group orders to multiple locations. Additional order forms may be obtained by contacting The Sheridan Press. **All orders must be received within 60 days of publication date or additional charges will apply.**

Prepayment or an institution purchase order is required to process your order. The online form will provide an invoice.

Delivery

Your order will be shipped within 3 weeks of the *Science* issue date. Allow extra time for delivery. If quicker delivery is necessary, please call for pricing and availability. UPS ground postage and handling are included in the prices (1-5 day delivery). Orders shipped to authors outside the continental US are mailed via an expedited air service at an additional charge. Orders for articles over 1 year past publication will require additional time to produce.

Corrections

If a serious error occurs in the published version of the paper, the error can be corrected in reprints if the editorial office is notified promptly. Please contact the editor or copy editor of your paper with the corrections.

Reprint Order Specifications

All reprints will include either a title page (in black and white or color, depending upon the type of reprint ordered) or the cover of *Science* from the issue in which your article appears. If the cover of *Science* is selected, there will be a \$100 additional fee (cover will appear in black & white or color, depending on the type of reprints ordered). This adds one page to the length of your paper.

Pricing

Reprint pricing is shown in the following tables. Orders are limited to 500 copies per author. To convert color articles to black & white reprints, add \$200. For articles over 12 months past publication, please contact The Sheridan Press for pricing. **This pricing is valid within 60 days of publication date.**

Black and White Reprints

Quantity	100	200	300	400	500
≤4 pages	300	350	395	435	470
≤8 pages	460	520	575	625	670
≤12 pages	600	665	725	780	830

Color Reprints

Quantity	100	200	300	400	500
≤4 pages	1800	1890	1960	2020	2070
≤8 pages	2140	2235	2310	2375	2430
≤12 pages	2485	2585	2665	2735	2795

Air Shipping Charges

(orders shipped outside the continental US only)

\$120 – 8 pages or less and 200 copies or less
 \$175 – More than 8 pages or more than 200 copies



Instructions for Handling PDF Galley Proofs

It is important that you return galley corrections within 48 hours directly to your copy editor. Please let your copy editor know immediately if there will be any delay.

Dear Author:

Thank you for publishing in *Science*. This letter explains how to mark this PDF file and transmit corrections to your galley proofs. This PDF file includes the following:

1. Instructions for ordering reprints and paying for use of color in figures (p. 1).
2. Detailed instructions for marking the proof (pp. 2-4)
3. Galley proofs of your paper (starting on p. 5).

If your manuscript contains color figures, the colors and resolution in the proofs may appear different from those of the final published figures. Our art department will send separate color figure proofs. Also, although your paper begins at the top of a page in the proofs, it may not when printed in *Science*.

A separate PDF file showing editorial changes to your paper has been, or shortly will be, e-mailed to you by your copy editor. Please use this in checking your proofs, but do not mark corrections on it.

In order to make galley corrections:

1. Please pay color figure charges online at www.sheridan.com/aaas/eoc. The same online form can be used to order reprints.
2. Mark all changes on the galley proofs (this file) directly using Acrobat Reader (free) v. X (available at: <http://get.adobe.com/reader/>).
3. Additional instructions for marking text are given on the next two pages. To start, select the Comment button on the upper right side of the Adobe Reader screen.
 - a. All edits of the text and text corrections should be made with "Text Edits" using insert, replace, or delete/cross out selections. *Please do not use sticky notes, comments, or other tools for actual text edits.*
 - b. You can control formatting (e.g., italics or bold) by selecting edited text.
 - c. Indicate edits to special or Greek characters with a comment. Use the "sticky note" for comments. Please refrain from using other tools.
 - d. Please collect all corrections into one file; import comments provided by multiple authors into one file only (Document menu/Comments/Import Comments).
 - e. Be sure to save the marked file and keep a copy.
4. Respond to all of the copy editor's queries listed at the end of the edited manuscript or as embedded PDF notes in the copyedited manuscript, by directly editing the galley text in the PDF with the annotation tools or using sticky notes on the galley PDF.
5. Check reference titles and additional supplementary references on the edited word file sent to you by your copyeditor. Address any edits here in the note back to your copyeditor.
6. Check all equations, special characters, and tables carefully. Check spelling of all author names for accuracy.
7. Make a copy of the corrected galley proofs for yourself. Return the corrected galley proofs to the *Science* copy editor as an attachment to an email.
8. If you cannot mark the proofs electronically, please e-mail a list of corrections to the copy editor.

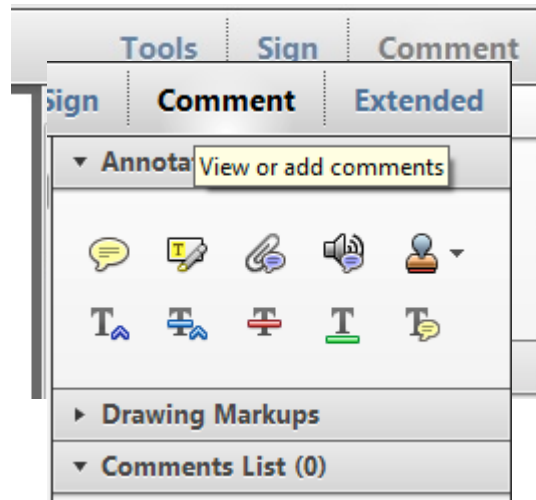
Thank you for your prompt attention,
The Editors

Instructions on how to annotate your galley PDF file using Adobe Acrobat Reader X

To view, annotate and print your galley, you will need Adobe Reader X. This free software can be downloaded from: <http://get.adobe.com/reader/>. It is available for Windows, Mac, LINUX, SOLARIS, and Android. The system requirements can also be found at this URL.

To make corrections and annotations in your galley PDF with Adobe Reader X, use the commenting tools feature, located by clicking **Comment** at the upper right of your screen. You should then see the Annotations Palette with the following annotation tools. (These tools can also be accessed through View>Comment>Annotations.

Although all the files from SPI will have these commenting tools available, occasionally this feature will not be enabled on a particular PDF. In these cases, you can use the two default commenting tools to annotate your files: Sticky Note and Highlight Text.



To start adding comments, select the appropriate commenting tool from the Annotation Palette.

TO INDICATE INSERT, REPLACE, OR REMOVE TEXTS

- **Insert Text**

Click the  button on the Commenting Palette. Click to set the cursor location in the text and start typing. The text will appear in a commenting box. You may also cut-and-paste text from another file into the commenting box.

- **Replace Text**

Click the  button on the Commenting Palette. To highlight the text to be replaced, click and drag the cursor over the text. Then type in the replacement text. The replacement text will appear in a commenting box. You may also cut-and-paste text from another file into this box.

- **Remove Text**

Click the  button on the Commenting Palette. Click and drag over the text to be deleted. The text to be deleted will then emphasize with a ~~strikethrough~~.

LEAVE A NOTE / COMMENT

- **Add Note to Text**

Click the  button on the Commenting Palette. Click to set the location of the note on the document and simply start typing. Kindly refrain from using this feature to make text edits

- **Add Sticky Note**

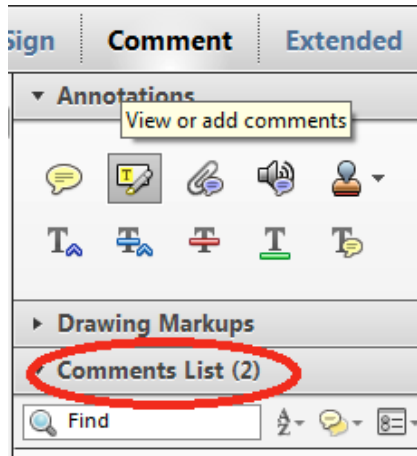
Click the  button on the Commenting Palette. Click to set the location of the note on the document and simply start typing. Kindly refrain from using this feature to make text edits

HIGHLIGHT TEXT / MAKE A COMMENT

- Click the  button on the Commenting Palette. Click and drag over the text. To make a comment, double click on the highlighted text and simply start typing.

REVIEW

All comments added in the active document are listed in **Comments List** Palette. Navigate by clicking on a correction in the list.



ATTACH A FILE

For equations, tables and figures that need to be added or replaced, or for a large section of text that needs to be inserted, users will find it better to just attach a file.

Click  button on the Commenting Palette. And then click on the figure, table or formatted text to be replaced. A window will automatically open allowing you to attach the file.

RESEARCH ARTICLE

IMMUNOLOGY

Liver type 1 innate lymphoid cells develop locally via an interferon- γ -dependent loop

Lu Bai^{1,2,*}, Margaux Vienne^{3,*}, Ling Tang^{1,2,*}, Yann Kerdiles^{3,*}, Marion Etiennot³, Bertrand Escalière³, Justine Galluso³, Haiming Wei^{1,2,4}, Rui Sun^{1,2,4,††}, Eric Vivier^{3,5,6,††}, Hui Peng^{1,2,4,††}, Zhigang Tian^{1,2,4,††}

The pathways that lead to the development of tissue-resident lymphocytes, including liver type 1 innate lymphoid cells (ILC1s), remain unclear. We show here that the adult mouse liver contains Lin⁻Sca-1⁺Mac-1⁺ hematopoietic stem cells derived from the fetal liver. This population includes Lin⁻CD122⁺CD49a⁺ progenitors that can generate liver ILC1s but not conventional natural killer cells. Interferon- γ (IFN- γ) production by the liver ILC1s themselves promotes the development of these cells in situ, through effects on their IFN- γ R⁺ liver progenitors. Thus, an IFN- γ -dependent loop drives liver ILC1 development in situ, highlighting the contribution of extramedullary hematopoiesis to regional immune composition within the liver.

Hematopoietic stem cells (HSCs) give rise to multiple lineages of progenitors. The predominant sites where hematopoiesis occurs change during the course of mouse and human development (1, 2). In mice, the first hematopoietic progenitors are found in the yolk sac 7 days post coitus (dpc) and lead to embryonic erythroid cells and myeloid cells (3). The first HSCs initially emerge in the aorta-gonad-mesonephros region of the embryo after 10.5 dpc (4). These cells then colonize the fetal liver at 11 dpc, subsequently expanding and differentiating. Before birth, fetal liver HSCs begin to seed the bone marrow (BM) (3). BM hematopoiesis has long been considered the major source of mature blood cells during adulthood, but extramedullary hematopoiesis in other adult organs, such as the liver and spleen, can occur under certain circumstances and makes a particularly important contribution when the BM is not functional (2). Moreover, several lines of evidence suggest that the adult liver environment remains compatible with hematopoiesis and contains a few HSCs with long-term capacity for hematopoietic reconstitution (5). However, the origin and contribution of adult liver hematopoietic progenitors to local immunological features remain unknown.

The immune composition of the liver differs from that of other organs, with a large number of resident innate immune cells such as type 1 innate lymphoid cells (ILC1s) (6, 7), $\gamma\delta$ T cells, and natural killer T (NKT) cells. Adult mouse liver ILCs include CD49a⁺CD49b⁺ conventional natural killer (cNK) cells and CD49a⁺CD49b⁻ ILC1s (8), which can be distinguished on the basis of differences in the expression of CD69, CD200R1, Eomes, T-bet, and TRAIL (fig. S1, A and B). In terms of effector function, liver CD49a⁺CD49b⁻ ILC1s produce larger amounts of tumor necrosis factor- α , generate smaller quantities of interferon- γ (IFN- γ) and perforin, and have similar levels of granzyme B as compared to CD49a⁻CD49b⁺ cNK cells, after stimulation with interleukin-12 (IL-12), IL-15, and IL-18 (fig. S1, C and D). However, the branch point at which the development of liver ILC1s separates from that of liver cNK cells remains unknown. Given the tissue-resident status of CD49a⁺CD49b⁻ ILC1s in the liver (9) and their impaired reconstitution in mice receiving BM transplants (6), we investigated whether liver ILC1s could develop from local hematopoietic progenitors during adulthood.

Adult mouse liver contains progenitors of liver-resident ILC1s

Previous studies have demonstrated that fetal liver HSCs are enriched in a lineage (Lin⁻) negative population expressing both Mac-1 and Sca-1 (10). By analyzing the expression of Mac-1 and Sca-1 on CD45⁺Lin⁻ progenitors from various tissues from wild-type (WT) mice, we found that, like the fetal liver, the adult liver contained CD45⁺Lin⁻Sca-1⁺Mac-1⁺ (LSM) cells, which were present at significantly higher frequencies than in adult BM, peripheral blood, and small intestine lamina propria (siLP) (Fig. 1, A and B, and fig. S2A). Like Lin⁻Sca-1⁺c-kit⁺ (LSK) BM HSCs, some adult liver LSM cells

expressed c-kit, but also Flt3 (CD135) and CD34, reminiscent of short-term HSCs (ST-HSCs) and multipotent progenitors, as well as CD93, which is strongly expressed by fetal liver HSCs (11) (Fig. 1C). In addition, unlike long-term HSCs (LT-HSCs) characterized as EPCR⁺CD150⁺CD48⁻ (12, 13), most of the adult liver LSM cells were EPCR⁺CD150⁻CD48⁺ (fig. S2B), and only a minor fraction (10 to 20%) expressed the medium-term HSC marker CD49b (14) (fig. S2B). Adult liver LSM cells also strongly expressed the tissue-resident marker CD49a but had low levels of the chemokine receptors CXCR3 and CXCR6 (fig. S2B). Consistent with their heterogeneous cell-surface phenotype, uniform manifold approximation and projection (UMAP) analysis of single-cell RNA sequencing (scRNA-seq) data for sorted LSM cells revealed 12 distinct cell clusters (fig. S3A and table S1). Using previously described hematopoietic progenitor signatures (15), we were able to identify cluster 9 as corresponding to LT-HSCs, cluster 2 as corresponding to ST-HSCs, and cluster 6 as corresponding to common lymphoid progenitors (fig. S3B). Notably, chimera experiments revealed that fetal liver cells reconstituted the pool of liver LSM cells (Fig. 1D) and ILC1s (Fig. 1E) more efficiently than BM cells. In addition, an analysis of parabiotic mice showed that adult liver LSM cells were strictly tissue resident at steady state (fig. S2, C and D). These experiments suggest that LSM cells contain fetal liver-derived multipotent hematopoietic populations, including progenitors that give rise to liver ILC1s. Consistent with this hypothesis, LSM cells purified from adult mouse liver and transferred into sublethally irradiated *Rag1*^{-/-} mice by portal-vein injection were able to generate multiple hematopoietic lineages (fig. S2E) and preferentially differentiated into CD49a⁺CD49b⁻ ILC1s rather than cNK cells in the recipient liver (Fig. 1F).

Analysis of liver ILC1 progenitor heterogeneity

We then sought to dissect the mechanisms by which adult liver LSM cells gave rise to liver ILC1s. In mice, Lin⁻NK1.1⁻CD49b⁻CD122⁺ cells have been described as BM progenitors that are able to generate NK cells in vitro and NK cells and T cells in vivo (16, 17). These cells, which do not express markers of mature cNK cells or liver ILC1s, were also detected in the liver of WT and LSM cell-recipient mice (Fig. 1, G and H). Unlike their counterparts from the BM and spleen, a large proportion of these cells expressed CD49a (Fig. 1, G and H). Liver CD49a⁺ or CD49a⁻Lin⁻CD122⁺ precursors from CD45.1⁺ mice were used for adoptive transfer into sublethally irradiated CD45.2⁺*Rag1*^{-/-} mice for a direct assessment of their developmental potential. Consistent with previous studies (17), both populations were able to generate B cells or T cells (fig. S2F). Both liver ILC1s and cNK cells could be generated from Lin⁻CD122⁺CD49a⁻

¹Hefei National Laboratory for Physical Sciences at Microscale, CAS Key Laboratory of Innate Immunity and Chronic Disease, School of Basic Medical Sciences, Division of Life Sciences and Medicine, University of Science and Technology of China, Hefei, China. ²Institute of Immunology, University of Science and Technology of China, Hefei, China. ³Aix Marseille Univ, CNRS, INSERM, CIML, Marseille, France. ⁴Research Unit for NK Cell Study, Chinese Academy of Medical Sciences, Beijing, China. ⁵APHM, Hôpital de la Timone, Marseille-ImmunoPole, Marseille, France. ⁶Innate Pharma, Marseille, France.

*These authors contributed equally to this work.

†These authors contributed equally to this work.

††Corresponding author. Email: vivier@ciml.univ-mrs.fr (E.V.); huipeng@mail.ustc.edu.cn (H.P.); sunr@ustc.edu.cn (R.S.); tgz@ustc.edu.cn (Z.T.)

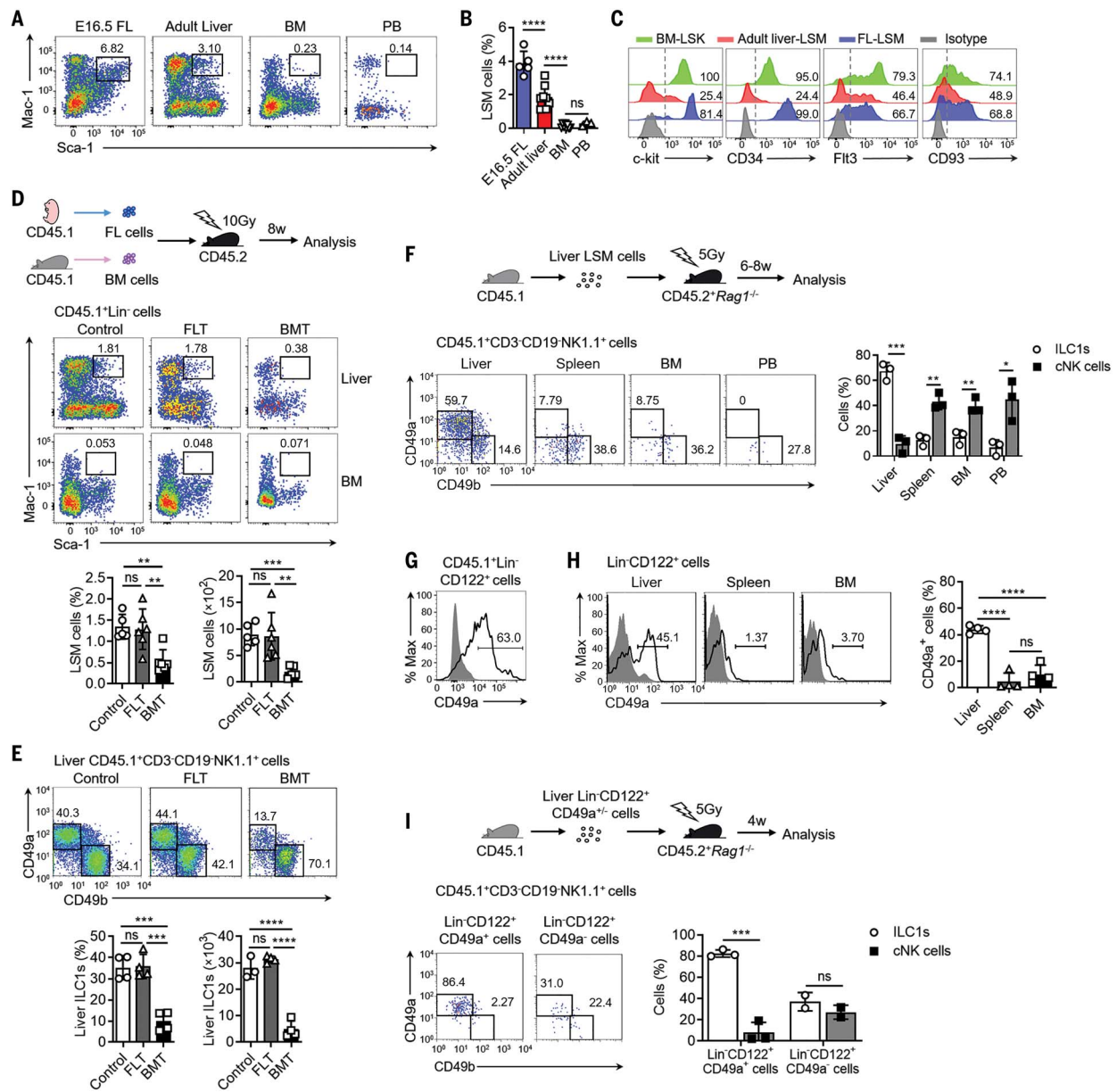


Fig. 1. Mouse liver contains hematopoietic progenitors producing liver-resident ILC1s. (A) Representative plots showing the expression of Sca-1 and Mac-1 on CD45⁺CD3⁺CD19⁺NK1.1⁺Gr-1⁻Ter-119⁻ (CD45⁺Lin⁻) cells from the embryonic day 16.5 (E16.5) fetal liver (FL), adult liver, adult bone marrow (BM), and peripheral blood (PB) of WT B6 mice. (B) Percentage of Sca-1⁺Mac-1⁺ cells among CD45⁺Lin⁻ cells from the indicated mouse tissues ($n = 3$ to 8 xxxxxxxx per group from one experiment representative of three independent experiments). (C) Representative histograms of c-kit, CD34, Flt3, and CD93 expression on CD45⁺Lin⁻Sca-1⁺Mac-1⁺ (LSM) cells from E16.5 to E16.5 fetal liver (blue) and adult liver (red). The expression of these markers on adult mouse BM CD45⁺Lin⁻Sca-1⁺c-kit⁺ (LSK) cells is shown as a control (green). (D and E) Lethally irradiated (10 Gy) CD45.2⁺ WT mice received 2×10^6 BM cells or E13.5 fetal liver cells from CD45.1⁺ WT mice and were analyzed 8 weeks after transfer ($n = 4$ to 6 per group from one experiment representative of two independent experiments). (D) Representative plots showing the expression of Sca-1 and Mac-1 on CD45.1⁺Lin⁻ cells from recipient liver and BM. (E) Representative plots showing the expression of CD49a and CD49b on CD45.1⁺CD3⁺CD19⁺NK1.1⁺ cells from the recipient liver. Percentage and absolute cell numbers of CD45.1⁺ LSM cells (D) or CD45.1⁺ ILC1s (CD3⁺CD19⁺NK1.1⁺CD49a⁺CD49b⁻) in the recipient liver (E) are indicated. FLT, fetal liver transfer; BMT, bone

marrow transfer. (F and G) Sublethally irradiated (5 Gy) CD45.2⁺Rag1^{-/-} mice that had received an adoptive transfer of 2500 adult liver LSM cells from CD45.1⁺ WT mice via hepatic portal-vein injection were analyzed 6 to 8 weeks after transfer ($n = 3$ per group from two independent experiments). (F) Representative plots showing the expression of CD49a and CD49b on CD45.1⁺CD3⁺CD19⁺NK1.1⁺ cells from the recipients and percentage of ILC1s and cNK cells among CD45.1⁺CD3⁺CD19⁺NK1.1⁺ cells. (G) Representative histogram showing CD49a expression on CD45.1⁺CD3⁺CD19⁺NK1.1⁺CD49b⁻CD122⁺ cells from the recipient liver. (H) Representative histograms and percentage of cells expressing CD49a among CD3⁺CD19⁺NK1.1⁺CD49b⁻CD122⁺ cells from the liver, spleen, and BM of WT mice ($n = 4$ per group from two independent experiments). (I) 4×10^4 CD49a⁺CD3⁺CD19⁺NK1.1⁺CD49b⁻CD122⁺ or CD49a⁺CD3⁺CD19⁺NK1.1⁺CD49b⁻CD122⁺ cells from the liver of CD45.1⁺ WT mice were transferred into sublethally irradiated CD45.2⁺Rag1^{-/-} mice, which were analyzed 4 weeks after transfer. Representative plots show the expression of CD49a and CD49b on CD45.1⁺CD3⁺CD19⁺ cells from liver recipients and the percentage of ILC1s and cNK cells among CD45.1⁺CD3⁺CD19⁺ cells ($n = 3$ per group from two independent experiments). Bar graphs show means \pm SDs [ANOVA tests [(B), (D), (E), and (H)] or t tests [(F) and (I)]; ns, not significant; * $P < 0.05$; ** $P < 0.01$; *** $P < 0.001$; **** $P < 0.0001$].

cells, whereas Lin⁻CD122⁺CD49a⁺ cells preferentially led to ILC1s and only minimal numbers of cNK cells (Fig. 1I). We characterized this progenitor population in more detail by performing scRNA-seq on sorted Lin⁻CD122⁺CD49a⁺ cells. Lin⁻CD122⁺CD49a⁺ cells presented almost the same pattern of clustering as that of LSM cells, but with a clear enrichment in clusters 3 and 5 (fig. S3A). Consistent with this, cytometry analysis indicated that a fraction of LSM cells had a Lin⁻CD122⁺CD49a⁺ cell phenotype and, conversely, a fraction of Lin⁻CD122⁺CD49a⁺ cells had a LSM phenotype, indicating a partial overlap between these two populations (fig. S3C). Nevertheless, the two major clusters of Lin⁻CD122⁺CD49a⁺ cells (clusters 3 and 5) presented an enrichment in the ILC1 signature relative to the cNK cell signature (fig. S3B). Heatmap analysis of the 20 most strongly expressed genes confirmed the assignment of clusters 2, 3, 5, 6, and 9 (fig. S3D). In particular, clusters 3 and 5 were characterized by the expression of genes related to both cNK cells and ILC1s, such as CD94 (*Klr1d1*) and genes of the NKG2 family (*Klrc1*, *Klre1*, and *Klre2*) (fig. S3D). Consistent with our observation that Lin⁻CD122⁺CD49a⁺ cells could generate T cells and with reported ILC1 transcriptomic signatures (18), clusters 3 and 5 displayed overall enrichment in the T cell signature, as illustrated by *Cd3d*, *Cd3e*, *Cd3g*, *Cd8a*, *Cd8b*, and *Cd2* (fig. S3, B and D). Pseudotime analysis proposed a trajectory extending from ST-HSC cluster 2 toward cluster 3 and then to cluster 5 of Lin⁻CD122⁺CD49a⁺ cells, suggesting that cluster 5 is the most restricted population of progenitors that generate liver ILC1s (fig. S3E). Thus, Lin⁻CD122⁺CD49a⁺ cells constitute a heterogeneous precursor population downstream from LSM cells, with a differentiation potential restricted to liver ILC1s rather than cNK cells.

IFN- γ signaling positively regulates the cellularity of liver ILC1s

We then investigated the factors involved in this extramedullary developmental pathway of liver ILC1s. *Ifng* deficiency results in low counts of liver CD3⁺NK1.1⁺ cells (19). We confirmed this finding by showing that *Ifng*-deficient (GKO) mice had a lower cell population-specific frequency and number of CD3⁺NK1.1⁺ ILC1s in the liver, but not in the spleen or BM (Fig. 2, A and B). Moreover, *Ifng* deficiency did not affect the numbers of other hepatic lymphocytes, such as B cells, $\gamma\delta$ T cells, CD4⁺ T cells, CD8⁺ T cells, and NKT cells (fig. S4A). Phenotypic analysis of liver CD3⁺NK1.1⁺ ILCs revealed that *Ifng* deficiency selectively reduced the frequency and number of liver ILC1s, defined as CD49a⁺CD49b⁻ or CD49a⁺Eomes⁻ cells (Fig. 2, C and D, and fig. S4B). Similar results were obtained in *Ifngr1*-deficient (GRKO) mice (Fig. 2E) and in mixed fetal liver chimera experiments, in

which fewer liver ILC1s were generated from GRKO than from WT donor cells (Fig. 2F). By contrast, siLP ILC1 and cNK cell numbers were similar in GKO mice and their WT counterparts (fig. S4D), indicating a selective impact of IFN- γ signaling on liver ILC1s. Phenotypic analyses did not reveal any differences in liver cNK cell or ILC1 maturation or activation status between *Ifng*-deficient and WT mice (fig. S5). We then assessed the effect of IFN- γ on liver ILC1 development by delivering a plasmid containing the IFN- γ cDNA to GKO mice via hydrodynamic tail-vein injection. High IFN- γ levels were maintained (Fig. 2G) and were accompanied by an increase in the frequency and number of liver ILC1s in GKO mice (Fig. 2, H and I). By contrast, liver cNK cell numbers increased transiently after injection but rapidly returned to normal levels (fig. S6). Thus, signaling through IFN- γ and its receptor positively regulate the cellularity of liver ILC1s.

IFN- γ signaling controls ILC1 development from intrahepatic hematopoietic progenitors

Despite the role of IFN- γ in the development of liver ILC1s, the IFN- γ receptors (including IFN- γ R1 and IFN- γ R2) were barely detectable on these cells (Fig. 3, A and B). By contrast, IFN- γ receptors were coexpressed by liver LSM cells but present at low to undetectable levels on BM LSK HSCs and on liver Lin⁻CD122⁺CD49a⁺ cells and ILC1s (Fig. 3, A and B). Consistent with these data, we observed that the frequencies of proliferative (Ki67⁺) LSM cells in the liver were lower in GKO mice than in WT mice (Fig. 3C). However, the frequencies of annexin V⁺ cells were similar across genotypes (Fig. 3C). By contrast, the hydrodynamic injection of the IFN- γ plasmid into GKO mice increased the numbers of liver LSM cells (Fig. 3D). Furthermore, the proliferation of ILC1s was not affected by *Ifng* deficiency (Fig. 3E). Additionally, in *Ncr1*^{Cre/+}*Ifngr1*^{fl/fl} mice, in which *Ifngr1* expression is conditionally abolished on NKp46⁺ cells, liver ILC1 numbers were unaffected by their lack of IFN- γ R1 (Fig. 3F). This observation was consistent with the weak or nonexistent expression of this receptor on mature ILC1s (Fig. 3, A and B). Finally, immunodeficient mice receiving equal numbers of GRKO and WT LSM cells presented liver ILC1s predominantly derived from WT donors (Fig. 3G). Thus, IFN- γ signaling promotes the expansion and differentiation of LSM cells but not of ILC1s, supporting a mechanistic model in which IFN- γ acts on these local progenitors to facilitate liver ILC1 development.

IFN- γ signaling promotes the intrahepatic development of liver ILC1s in a T-bet-dependent manner

Previous studies have shown a strict requirement of T-bet (encoded by the *Tbx21* gene) for

ILC1 development (7). We adoptively transferred equal numbers of *Tbx21*-deficient (CD45.2⁺) and WT (CD45.1⁺CD45.2⁺) fetal liver cells into lethally irradiated CD45.1⁺ mice. Most of the ILC1s in the livers of recipients were derived from the WT rather than the *Tbx21*-deficient donor (fig. S7A). Thus, T-bet acts as an intrinsic factor that governs liver ILC1 development. As assessment of T-bet expression by CD45⁺Lin⁻ progenitors revealed that, regardless of IFN- γ production, T-bet was expressed by a subset of CD45⁺Lin⁻ liver cells but rarely by phenotypically similar cells in the BM and spleen (fig. S7, B and C). We investigated the relationship between IFN- γ signaling and T-bet during ILC1 development in more detail, by culturing T-bet-deficient and WT fetal liver cells in the presence or absence of IFN- γ . The addition of IFN- γ to the culture system significantly promoted the generation of CD49a⁺CD49b⁻ ILC1s from WT fetal liver cells but had no effect on CD49a⁺CD49b⁺ cNK cell production (fig. S7, D and E), consistent with the results obtained in vivo. However, *Tbx21*-deficient fetal liver cells failed to generate ILC1s, even after stimulation with IFN- γ (fig. S7, D and E). Furthermore, the overexpression of IFN- γ in *Tbx21*-deficient mice via hydrodynamic injection failed to restore the frequency and number of liver ILC1s (fig. S7, F and G), further confirming that T-bet is required for IFN- γ -promoted liver ILC1 development from progenitors in situ. The frequency and number of LSM cells were higher in *Tbx21*-deficient mice, as was the level of IFN- γ receptor expression (fig. S7, H to K). Thus, T-bet is not required for LSM cell development. Furthermore, *Tbx21* deficiency impedes LSM cell differentiation into ILC1s.

IFN- γ produced by ILC1s promotes their development in the liver

We then studied multiple mouse models with deficiencies of specific cell populations to explore the cellular source of IFN- γ that affects liver ILC1 production. ILC1 numbers were unaffected in the absence of T or B cells in *Cd4*^{-/-}, *Cd8*^{-/-}, and μ MT-deficient mice (fig. S8). We therefore investigated whether the production of IFN- γ by the liver ILCs themselves was involved in the development of liver ILC1s. We generated mice with a conditional ablation of the *Ifng* gene in NKp46⁺ cells (Fig. 4, A and B, and fig. S9). Notably, *Ncr1*^{Cre/+}*Ifng*^{fl/fl} mice harbored a selective deficiency of liver ILC1s, with no change in the numbers of liver cNK cells or of other hepatic lymphocytes or siLP ILC1s (Fig. 4, C and D, and fig. S4, C and E). A selective lack of IFN- γ production by NKp46⁺ cells therefore reproduced the selective deficiency of liver ILC1s observed in total IFN- γ deficiency, indicating that IFN- γ derived from NKp46⁺ cells controls the production of ILC1s. We previously demonstrated that conditional

F2

F3

F4

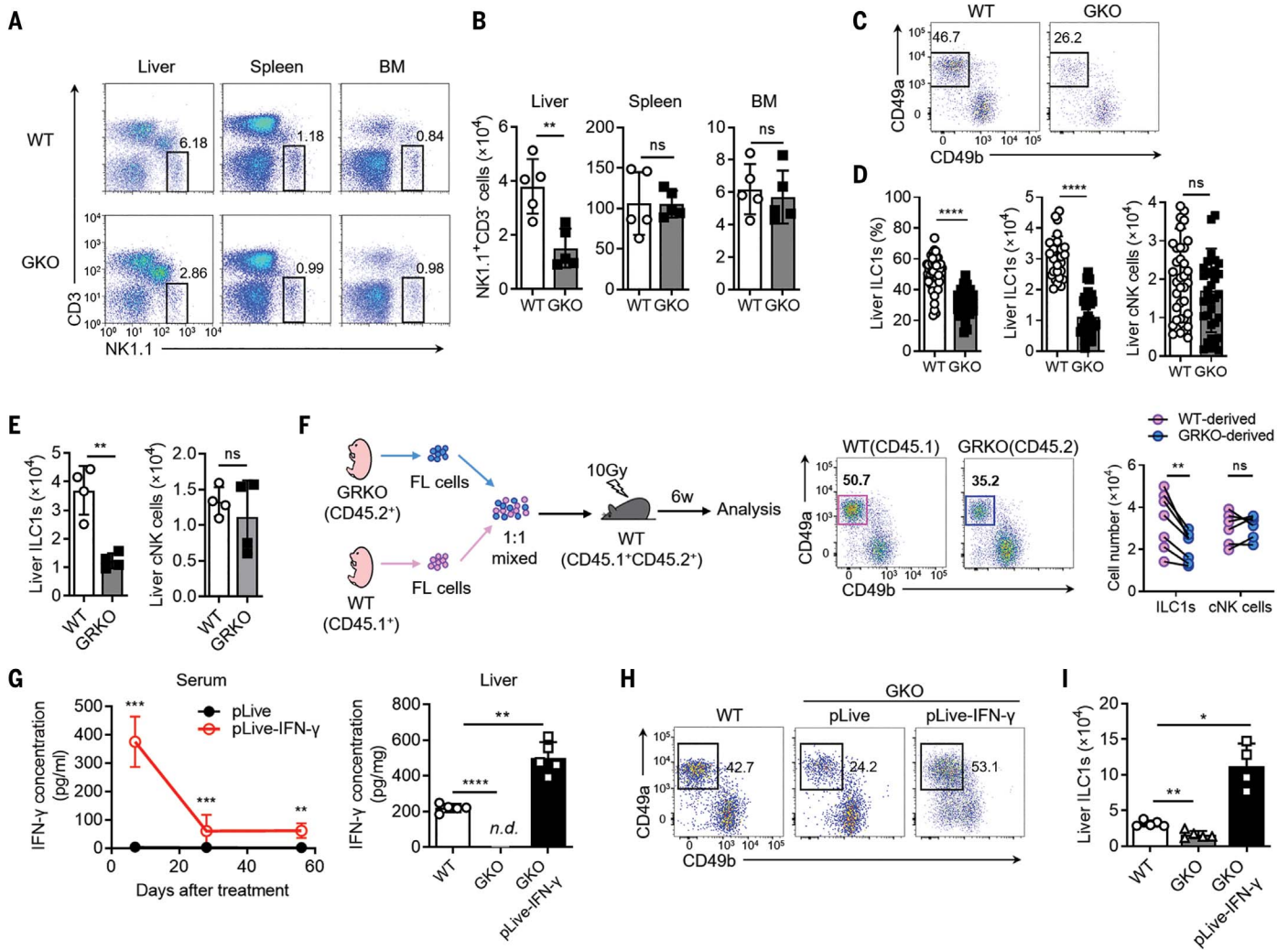


Fig. 2. IFN- γ signaling is required for liver ILC1 development. (A and B) Representative plots (A) and absolute cell numbers (B) of NK1.1⁺CD3⁻ cells in the indicated organs of WT and IFN- γ -knockout (GKO) mice ($n = 5$ per group from one experiment representative of at least three independent experiments). (C) Representative plots showing CD49a and CD49b expression on NK1.1⁺CD3⁻ cells in the liver of WT and GKO mice. (D) Percentage (among CD3⁻NK1.1⁺ cells) of liver ILC1s (CD3⁻NK1.1⁺CD49a⁺CD49b⁻) and absolute cell numbers for liver ILC1s and cNK cells (CD3⁻NK1.1⁺CD49a⁻CD49b⁺) in WT and GKO mice ($n = 28$ to 34 per group from at least three independent experiments). (E) Absolute cell numbers for ILC1s (left) and cNK cells (right) in the liver of WT and IFN- γ R1-deficient (GRKO) mice ($n = 4$ per group from one experiment representative of two independent experiments). (F) Lethally irradiated CD45.1⁺CD45.2⁺ WT mice received 10⁶ fetal liver cells from GRKO mice (CD45.1⁺CD45.2⁺) mixed with 10⁶ fetal liver cells from WT mice (CD45.1⁺CD45.2⁻) and were analyzed 6 weeks after transfer (left).

Representative plots showing the expression of CD49a and CD49b on GRKO donor-derived and WT donor-derived CD3⁻NK1.1⁺ cells in the liver of recipients (middle) and absolute cell numbers for GRKO donor-derived and WT donor-derived liver ILC1s from recipients (right) ($n = 6$ to 7 per group from one experiment representative of two independent experiments). (G) IFN- γ levels in the serum and liver tissue homogenate from WT mice and GKO mice after a hydrodynamic injection of 5 μ g pLive-IFN- γ or pLive control plasmid (60 days after injection for the liver tissue) ($n = 5$ per group from one experiment representative of two independent experiments). (H and I) Representative plots (H) showing the expression of CD49a and CD49b on liver CD3⁻NK1.1⁺ cells and absolute cell numbers for liver ILC1s (I) in mice 60 days after treatment, as described in (G) ($n = 5$ per group from one experiment representative of two independent experiments). Bar graphs depict means \pm SDs {ANOVA tests [(G) and (I)] or t tests [(B), (D), and (E)]; ns, not significant; * $P < 0.05$; ** $P < 0.01$; *** $P < 0.001$; **** $P < 0.0001$ }.

Eomes deficiency in NKp46⁺ ILCs leads to an absence of cNK cells, with no impact on liver ILC1s (20), ruling out a role for cNK cells in liver ILC1 development. Because all NKp46⁺ ILCs that produce IFN- γ are either cNK cells or ILC1s, IFN- γ production by ILC1s therefore promotes the development of ILC1s in the liver through its action on their progenitors.

Conclusion

The recent discovery of ILC1s has led to numerous studies showing that, in addition to its common properties, the phenotype of this population is organ specific, even at steady state (6, 7, 21). Liver ILC1s constitute a distinctive population among the diverse ILCs. Indeed, as opposed to salivary gland or uterus

ILC1s, liver ILC1s are not dependent on *Eomes* for their development (21) and have a selective requirement for the transcription factor *Hobit* (22). As a possible explanation for the particular phenotype of liver ILC1s, we show here that fetal liver-derived tissue-resident LSM hematopoietic cells are present specifically in the adult liver and include cells with the potential

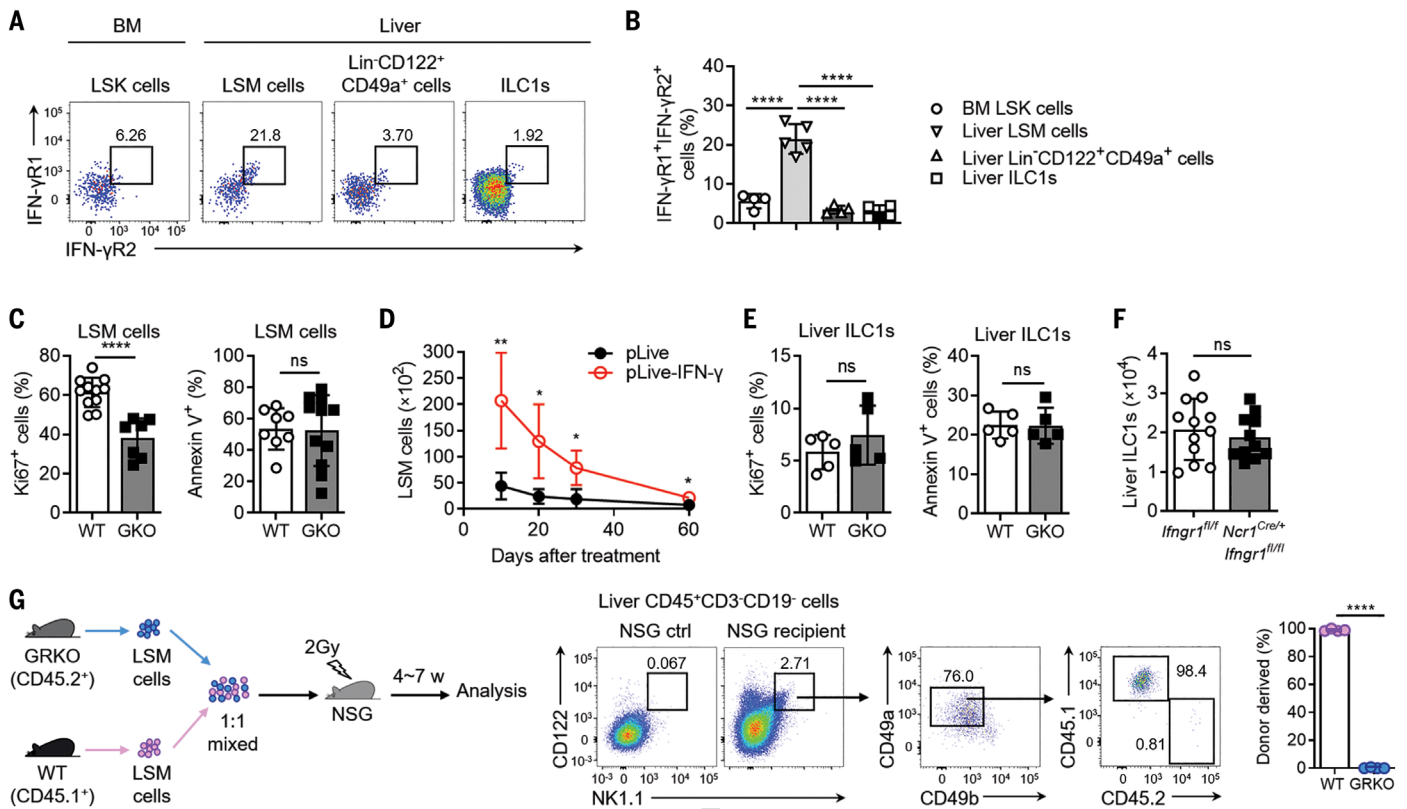


Fig. 3. IFN- γ signaling controls ILC1 development from intrahepatic hematopoietic progenitors. (A and B) Representative plots (A) and percentages (B) for the expression of IFN- γ R1 and IFN- γ R2 on BM LSK cells, liver LSM cells, liver Lin⁻CD122⁺CD49a⁺ cells, and liver ILC1s of adult WT mice ($n = 4$ per group from one experiment representative of two independent experiments). (C) Percentage of Ki67⁺ or AnnexinV⁺AAD⁻ cells among the liver LSM cells of WT and GKO mice ($n = 7$ to 11 per group from three independent experiments). (D) Absolute numbers of liver LSM cells at various time points after the hydrodynamic injection of 5 μ g of pLive-IFN- γ or pLive control plasmid into GKO mice ($n = 4$ to 5 per group from one experiment representative of two independent experiments). (E) Percentage of Ki67⁺ or AnnexinV⁺AAD⁻ cells

among the liver ILC1s of WT and GKO mice ($n = 5$ per group from one experiment representative of two independent experiments). (F) Absolute cell numbers for liver ILC1s in *Ifngr1^{fl/fl}* and *Ncr1^{Cre/+}Ifngr1^{fl/fl}* mice ($n = 12$ per group from three independent experiments). (G) Irradiated (2 Gy) NSG mice received equal numbers of GRKO (CD45.1⁻CD45.2⁺) LSM cells and WT (CD45.1⁺CD45.2⁻) LSM cells and were analyzed 4 to 7 weeks after transfer (left). Representative plots show donor-derived liver ILC1s in recipient mice (middle) and percentages of GRKO donor- and WT donor-derived liver ILC1s among recipient liver ILC1s (right) ($n = 4$ per group from two independent experiments). Bar graphs depict means \pm SDs {ANOVA test (B) or t tests [(C), (E), (F), and (G)]; ns, not significant; * $P < 0.05$; ** $P < 0.01$; **** $P < 0.0001$ }.

to generate liver ILC1s via an IFN- γ -dependent pathway. Besides the well-known roles of IFN- γ in innate and adaptive immunity to intracellular infections and in tumor control, there is growing evidence for a role of IFN- γ in regulating cell differentiation and homeostasis. In addition to its capacity to regulate the differentiation and proliferation of T helper 1 cells (23), IFN- γ also affects B cell and myeloid cell differentiation and maturation (24). However, it remains unclear whether hematopoietic progenitors are also affected by IFN- γ . Both stimulatory and suppressive effects of IFN- γ on hematopoietic homeostasis have been reported. IFN- γ has a negative effect on the maintenance of human CD34⁺CD38⁻ HSCs, by promoting their differentiation, rather than self-renewal (25). The maintenance of murine HSCs has also been reported to be inhibited by IFN- γ through the impairment of HSC proliferation in vitro (26), but in mycobacterial infection models, increases in HSCs were found to be dependent on IFN- γ

(27). We show here that the IFN- γ produced by liver ILC1s promotes their own development, through effects on the proliferation of their progenitor cells. Our data also provide mechanistic insights into the role of IFN- γ in this process. First, the presence of ILC1 progenitors in the liver, in contrast to the presence of cNK cell progenitors in the BM, is consistent with the preferential action of liver IFN- γ on ILC1s in situ. Second, IFN- γ positively supports ILC1 differentiation, as LSM cells express the IFN- γ receptors, and this signaling pathway is active in these cells. This finding is supported by scRNA-seq analysis, which revealed that IFN- γ -induced genes [such as interferon regulatory factor (*Irf*) 1 and *Irf*2, signal transducer and activator of transcription 1 (*Stat1*), *Cd44*, and beta-2 microglobulin (*B2m*)] are expressed in these cells (fig. S10). Finally, IFN- γ signaling promotes the expansion and differentiation of LSM cells, but not of ILC1s, in a Tbet-dependent manner. However, the mechanisms

by which ILC1-derived IFN- γ supports ILC1 differentiation, whereas cNK cell-derived IFN- γ does not, remain to be determined. It is tempting to speculate that microanatomic factors in the liver maintain ILC1 progenitors and their progeny in the same niches, but we were unable to test this hypothesis owing to a lack of tools for the reliable localization of ILC1 progenitors, ILC1s, and cNK cells in liver tissues. The liver contextual information underlying steady-state IFN- γ production by ILC1s also remains to be determined, together with the other pathways or cytokines potentially involved in liver ILC1 differentiation. Indeed, in the absence of IFN- γ , we observed a decrease in the number of liver ILC1s but not the total disappearance of these cells, indicating that IFN- γ acts in an amplification loop of liver ILC1 development in which other factors are also required.

Our findings reveal the contribution of extramedullary hematopoiesis to specialized immune cell origins and a distinctive regional

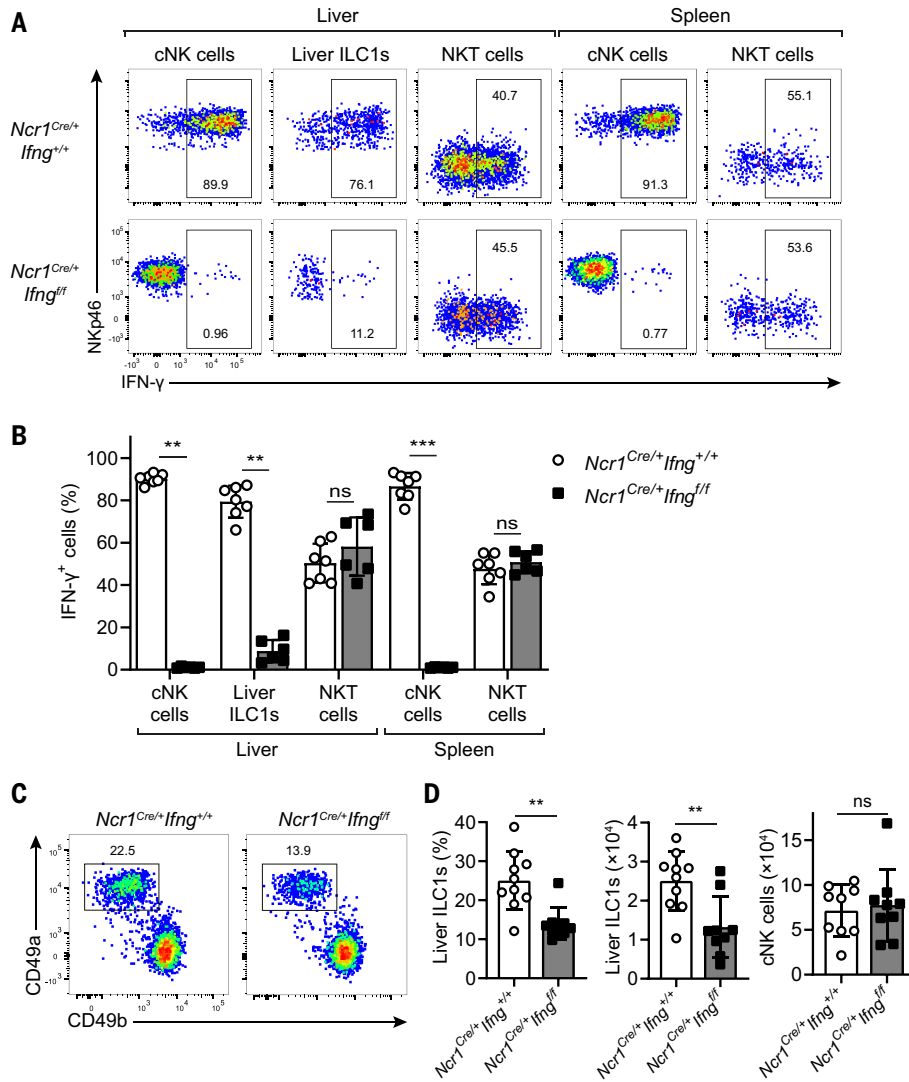


Fig. 4. Requirement of the IFN- γ produced by NKp46⁺ cells in liver ILC1 development. (A and B) Representative plots (A) and percentages (B) of IFN- γ ⁺ cells among WT (*Ncr1*^{Cre/+}*Ifng*^{+/+}) and IFN- γ -conditional knockout (*Ncr1*^{Cre/+}*Ifng*^{fl/fl}) liver and spleen cells after 4 hours of stimulation with IL-12 and IL-18 ($n = 7$ per group from two independent experiments). (C and D) Representative plots (C) showing CD49a versus CD49b expression on NKp46⁺NK1.1⁺ cells in the liver of *Ncr1*^{Cre/+}*Ifng*^{+/+} and *Ncr1*^{Cre/+}*Ifng*^{fl/fl} mice. Percentages (D) (among TCR β ⁺NKp46⁺NK1.1⁺ cells) and absolute numbers of liver ILC1s and cNK cells from *Ncr1*^{Cre/+}*Ifng*^{+/+} and *Ncr1*^{Cre/+}*Ifng*^{fl/fl} mice ($n = 9$ per group from three independent experiments). Bar graphs depict means \pm SDs (t tests; ns, not significant; ** $P < 0.01$; *** $P < 0.001$).

immune feature within the liver. These results are reminiscent of the local development of macrophages from embryonic precursors that selectively seed the tissues (28, 29) and of the in situ differentiation of lung ILC2s from tissue-resident progenitors (30, 31). They extend our knowledge of the importance of extramedullary hematopoiesis to cells of lymphoid origin.

Materials and methods

Mice

WT C57BL/6 (B6) mice were purchased from the Shanghai Experimental Animal Center. *Ifng*^{fl/fl} (GRKO) and *Rag1*^{-/-} mice were purchased from GemPharmatech Co., Ltd (Nanjing, China). CD45.1⁺

mice (002014), *Tbx21*^{-/-} mice (004432), and *Ifngr1*^{fl/fl} (025394) mice were purchased from The Jackson Laboratory. The *Ncr1*^{Cre} mice were generated as previously described (32). *Ifng*^{-/-} (GKO) mice (33) were provided by S. Su (Shantou University, Shantou, China). *Cd4*^{-/-} mice (34), *Cd8*^{-/-} mice (34), and μ MT-deficient mice (35) were provided by Z. Lian (South China University of Technology, Guangzhou, China). CD45.1⁺CD45.2⁺ mice and *Ncr1*^{Cre}*Ifngr1*^{fl/fl} mice were bred in-house. The *Ifng*^{fl/ox} mice were a gift from A. Tedgui (Paris Cardiovascular Research Center, France). No abnormalities were detected in terms of the reproduction, development and life span of *Ncr1*^{Cre/+}*Ifng*^{fl/fl} mice in SPF housing conditions.

The mice described above all have a B6 background. NSG mice (Balb/c background) were purchased from Shanghai Model Organisms Center, Inc. All mice were maintained under specific pathogen-free conditions, in accordance with the guidelines for the handling and care of experimental animals at the University of Science and Technology of China and with French and European guidelines for animal care.

Cell preparation

Liver mononuclear cells (MNCs) were isolated with a slightly modified version of a previously described method (36). Briefly, livers were collected and passed through a 200-gauge stainless steel mesh. The cells were then isolated by gradient centrifugation with 40 and 70% Percoll. Splenocytes and fetal liver cells were isolated by forcing the tissues through a stainless steel mesh and lysing erythrocytes. The BM cells were obtained by flushing femurs and then lysing erythrocytes. The isolation of siLP lymphocytes was performed as previously described (37, 38). Briefly, the small intestine was resected and cleaned of residual fat tissue. Peyer's patches were removed and the intestine was cut open longitudinally and washed in ice-cold phosphate-buffered saline (PBS). The small intestine tissue was then incubated in PBS containing 5% fetal bovine serum (Gibco), 5 mM ethylenediaminetetraacetic acid (EDTA; Sinopharm), and 15 mM 4-(2-hydroxyethyl)-1-piperazineethanesulfonic acid (HEPES; BBI Life Sciences) for 60 min with shaking at 37°C. The supernatant was discarded and the remaining tissue was further cut into small pieces and incubated at 37°C for 2 hours with shaking in Iscove's Modified Dulbecco's Medium (IMDM) (HyClone) with 1 mg/ml Collagenase IV (Sigma) and 0.5 mg/ml DNase I (Sigma). The supernatant was collected after each incubation step, and the preparation was further enriched in lymphocytes by Percoll gradient centrifugation.

Sorting and adoptive transfer

For studies of the development of liver ILC1s, fetal liver cells from 13.5-day-old fetuses or adult BM cells were used for adoptive transfer into lethally irradiated [10 Gy] administered 1 day before adoptive transfer] mice via tail-vein injection. We studied the development potential of liver LSM cells and CD49a⁺ ILC1s, by sorting CD45⁺Lin⁻Sca-1⁺Mac-1⁺ (LSM) cells, CD49a⁺CD122⁺NK1.1⁻CD3⁻CD19⁻ cells, and CD49a⁻CD122⁺NK1.1⁻CD3⁻CD19⁻ cells from adult CD45.1⁺ mice and using these cells for adoptive transfer into sublethally irradiated (5 Gy administered 1 day before adoptive transfer) *Rag1*^{-/-} mice via hepatic portal vein injection. We evaluated the effect of IFN- γ signaling on LSM cell development potential, by purifying LSM cells from adult GRKO and CD45.1⁺ mice, and transferring them into 2

Gy-irradiated NSG mice via tail-vein injection. Cell populations were purified on a FACS Aria II Cell Sorter or FACS Aria Fusion (BD Biosciences).

Cell cultures

The generation of NK cells from fetal liver cells can be reproduced in vitro in a two-step procedure, as described for multipotent stem cells (39, 40). On day 0, fetal liver cells from 13.5-day-old fetuses were cultured at a density of 10^6 cells per well in complete Roswell Park Memorial Institute (RPMI) medium supplemented with 5% fetal bovine serum (GIBCO), 30 ng/ml mouse SCF (stem cell factor, PeproTech), 10 ng/ml mouse Flt3L (PeproTech), and 0.5 ng/ml mouse IL-7 (PeproTech), with or without 20 ng/ml mouse IFN- γ (PeproTech). Cells received fresh supplemented medium on day 3 to stimulate their differentiation into NK cell progenitors. On day 5, cells were collected and cultured on a confluent monolayer of OP9 stromal cells in complete RPMI medium supplemented with 5% fetal bovine serum and 30 ng/ml mouse IL-15 (PeproTech). On day 8, cells were re-fed with the same medium to promote the generation of mature NK cells. On day 10, cells were collected and analyzed by flow cytometry. For ex vivo cell stimulation, liver and spleen mononuclear cells were incubated with IL-12 (25 ng/ml; eBiosciences), IL-18 (20 ng/ml; MBL International), or PMA (200 ng/ml; Sigma), ionomycin (1 μ g/ml; Sigma), and protein transport inhibitor GolgiPlug (BD Biosciences) for 4 hours. We compared the expression of effector molecules between liver ILC1s and cNK cells, by culturing liver mononuclear cells with IL-12 (10 ng/ml; Peprotech), IL-15 (10 ng/ml; Peprotech), and IL-18 (50 ng/ml; R&D) for 18 hours, with the addition of monensin (2.5 μ g/ml; Sigma-Aldrich) for the last 4 hours. Purified liver ILC1s or cNK cells were plated at a density of 5×10^4 cells per well in 96 well-plates, and cells were cultured with IL-12 (10 ng/ml; Peprotech), IL-15 (10 ng/ml; Peprotech), and IL-18 (50 ng/ml; R&D) for 24 hours. The culture supernatant was collected for determinations of the concentration of granzyme B.

scRNA-seq

Purified liver LSM cells and Lin⁻CD122⁺CD49a⁺ cells from adult WT mice were stained with 0.4% Trypan blue to check their viability (>90% before processing for scRNA-seq). Sequencing libraries were prepared with randomly interrupted whole-transcriptome amplification products, to enrich the 3' end of the transcripts linked to the cell barcode and UMI. Library construction was performed according to the manufacturer's standard protocol (CG000206 Rev D, 10X Genomics). Sequencing libraries were quantified with a High Sensitivity DNA Chip (Agilent) on a Bioanalyzer 2100 and with the Qubit High Sensitivity DNA Assay (Thermo Fisher Scientific).

The libraries were sequenced on a NovaSeq6000 (Illumina). Reads were processed with the Cell Ranger 2.1.0 pipeline, using the default and recommended parameters. FASTQs generated from the Illumina sequencing output were aligned with the mouse genome, version GRCh38, with the STAR algorithm. Gene-barcode matrices were then generated for each individual sample by counting UMIs and filtering non-cell-associated barcodes. Finally, we generated a gene-barcode matrix containing the barcoded cells and gene expression counts. This output was then imported into the Seurat (v2.3.0) R toolkit (41) for quality control and downstream analysis of our scRNA-seq data. LSM cell and Lin⁻CD122⁺CD49⁺ cell samples were first analyzed separately. Low-quality cells were excluded in an initial quality-control (QC) step, by removing cells expressing genes expressed in fewer than three cells, cells expressing fewer than 200 genes, and cells expressing more than 3000 genes. Cells with more than 5% mitochondrial-associated expressed genes or with less than 15% ribosome-associated expressed genes were also removed. QC resulted in 2930 LSM cells and 1208 Lin⁻CD122⁺CD49⁺ cells being retained for further analysis. Library-size normalization was performed on the UMI-collapsed gene expression values for each cell barcode, by scaling by the total number of transcripts and multiplying by 10,000. The data were then log-transformed before further downstream analysis with Seurat (3.1.5) (41). We first selected genes with a high variance, using the FindVariableGenes function with the "vst" method and nfeatures set to 2000. We then reduced the dimensionality of our data by principal component analysis (PCA) and performed clustering with the FindNeighbors and FindClusters functions (20 pcs and a resolution of 0.5). For visualization, we applied RunUMAP, using 20 pcs. We then integrated the samples with the FindIntegrationAnchors function, using "cca" as a reduction parameter, and IntegrateData function, using 30 pcs for both of them. Clustering was performed with the FindNeighbors and FindClusters functions, using 30 pcs and a resolution of 0.4. We identified cluster markers with FindMarkers, with the parameter only.pos set to TRUE, to obtain only genes up-regulated relative to all other cells for use as markers. Marker genes were defined as genes with an adjusted *P*-value <0.05 tested in a non-parametric Wilcoxon rank-sum test. ST-HSC, LT-HSC, and CLP scores were calculated using previously published signatures (15). Liver ILC1 and cNK cell scores were calculated with gene signatures extracted from previously published microarray data for liver ILC1s and cNK cells (18). The T cell signature was composed of genes with a correlation coefficient of more than 0.75 with the *Terb-1* gene in biogps (<http://biogps.org/>). Module scores for these signatures were calculated with the AddModuleScore function from Seurat. Pseudotime analysis was performed with the

Monocle3 package (0.2.3). The start of the trajectory was set to the cluster with the highest ST-HSC signature score.

Antibody staining and flow cytometry

The antibodies listed in table S2 were used for flow cytometry. AnnexinV were purchased from BD Biosciences (San Jose, CA). Cells were incubated with rat serum for 30 min to block Fc receptors, and then stained with fluorescently labeled monoclonal antibodies (mAbs). Intracellular cytokine and transcriptional factors were stained with the BD Cytofix/Cytoperm Fixation/Permeabilization Kit or the Foxp3 staining kit (eBioscience). Data were collected on a flow cytometer (LSR II and LSRFortessa; BD) and analyzed with FlowJo V10 software.

Plasmids

Mouse *Ifng* cDNA was inserted into the pLive vector (Mirus Bio) to force gene expression under the control of the mouse albumin promoter. Mice overexpressing IFN- γ were established by intravenously injecting 5 μ g of pLive-IFN- γ plasmid dissolved in 2 ml of PBS into mice over a period of 5 to 6 s.

Enzyme-linked immunosorbent assay

IFN- γ levels in serum were measured with mouse IFN- γ ELISA kits according to the manufacturer's instructions (DAKEWE). Granzyme B levels in the culture supernatant were determined with mouse granzyme B ELISA kits, according to the manufacturer's instructions (Multisciences).

Parabiosis

Parabiosis was performed as previously described (6, 21). Briefly, a longitudinal incision was made along the lateral surface of adult CD45.2⁺ (WT or GRKO) and CD45.1⁺ WT mice. The mice were then joined at the elbow and knee with dissolvable sutures and the incision was closed. After surgery, the mice were administered an antibiotic [sulfamethoxazole and trimethoprim (Sulfatrim)] solution for 14 days.

Statistical analysis

The statistical significance of differences was determined in Student's *t* tests or analysis of variance (ANOVA) tests with Brown-Forsythe and Welch corrections when required. The statistical analysis in fig. S3 was performed with Dunn's test. Differences with a *P*-value <0.05 were considered statistically significant.

REFERENCES AND NOTES

1. J. Seita, I. L. Weissman, Hematopoietic stem cell: Self-renewal versus differentiation. *WIREs Syst. Biol. Med.* 2, 640–653 (2010). doi: 10.1002/wsbm.86; pmid: 20890962
2. C. H. Kim, Homeostatic and pathogenic extramedullary hematopoiesis. *J. Blood Med.* 1, 13–19 (2010). doi: 10.2147/JBM.S7224; pmid: 22282679
3. H. K. A. Mikkola, S. H. Orkin, The journey of developing hematopoietic stem cells. *Development* 133, 3733–3744 (2006). doi: 10.1242/dev.02568; pmid: 16968814

4. A. Medvinsky, E. Dzierzak, Definitive hematopoiesis is autonomously initiated by the AGM region. *Cell* **86**, 897–906 (1996). doi: [10.1016/S0092-8674\(00\)80165-8](https://doi.org/10.1016/S0092-8674(00)80165-8); pmid: [8808625](https://pubmed.ncbi.nlm.nih.gov/8808625/)
5. H. Taniguchi, T. Toyoshima, K. Fukao, H. Nakauchi, Presence of hematopoietic stem cells in the adult liver. *Nat. Med.* **2**, 198–203 (1996). doi: [10.1038/nm0296-198](https://doi.org/10.1038/nm0296-198); pmid: [8574965](https://pubmed.ncbi.nlm.nih.gov/8574965/)
6. H. Peng et al., Liver-resident NK cells confer adaptive immunity in skin-contact inflammation. *J. Clin. Invest.* **123**, 1444–1456 (2013). doi: [10.1172/JCI66381](https://doi.org/10.1172/JCI66381); pmid: [23524967](https://pubmed.ncbi.nlm.nih.gov/23524967/)
7. C. Daussey et al., T-bet and Eomes instruct the development of two distinct natural killer cell lineages in the liver and in the bone marrow. *J. Exp. Med.* **211**, 563–577 (2014). doi: [10.1084/jem.20131560](https://doi.org/10.1084/jem.20131560); pmid: [24516120](https://pubmed.ncbi.nlm.nih.gov/24516120/)
8. E. Vivier et al., Innate Lymphoid Cells: 10 Years On. *Cell* **174**, 1054–1066 (2018). doi: [10.1016/j.cell.2018.07.017](https://doi.org/10.1016/j.cell.2018.07.017); pmid: [30142344](https://pubmed.ncbi.nlm.nih.gov/30142344/)
9. G. Gasteiger, X. Fan, S. Dikiy, S. Y. Lee, A. Y. Rudensky, Tissue residency of innate lymphoid cells in lymphoid and nonlymphoid organs. *Science* **350**, 981–985 (2015). doi: [10.1126/science.aac9593](https://doi.org/10.1126/science.aac9593); pmid: [26472762](https://pubmed.ncbi.nlm.nih.gov/26472762/)
10. S. J. Morrison, H. D. Hemmati, A. M. Wandycz, I. L. Weissman, The purification and characterization of fetal liver hematopoietic stem cells. *Proc. Natl. Acad. Sci. U.S.A.* **92**, 10302–10306 (1995). doi: [10.1073/pnas.92.22.10302](https://doi.org/10.1073/pnas.92.22.10302); pmid: [7479772](https://pubmed.ncbi.nlm.nih.gov/7479772/)
11. C. T. Jordan et al., Long-term repopulating abilities of enriched fetal liver stem cells measured by competitive repopulation. *Exp. Hematol.* **23**, 1011–1015 (1995). pmid: [7635180](https://pubmed.ncbi.nlm.nih.gov/7635180/)
12. M. J. Kiel et al., SLAM family receptors distinguish hematopoietic stem and progenitor cells and reveal endothelial niches for stem cells. *Cell* **121**, 1109–1121 (2005). doi: [10.1016/j.cell.2005.05.026](https://doi.org/10.1016/j.cell.2005.05.026); pmid: [15989959](https://pubmed.ncbi.nlm.nih.gov/15989959/)
13. A. B. Balazs, A. J. Fabian, C. T. Esmen, R. C. Mulligan, Endothelial protein C receptor (CD201) explicitly identifies hematopoietic stem cells in murine bone marrow. *Blood* **107**, 2317–2321 (2006). doi: [10.1182/blood-2005-06-2249](https://doi.org/10.1182/blood-2005-06-2249); pmid: [16304059](https://pubmed.ncbi.nlm.nih.gov/16304059/)
14. P. Benveniste et al., Intermediate-term hematopoietic stem cells with extended but time-limited reconstitution potential. *Cell Stem Cell* **6**, 48–58 (2010). doi: [10.1016/j.stem.2009.11.014](https://doi.org/10.1016/j.stem.2009.11.014); pmid: [20074534](https://pubmed.ncbi.nlm.nih.gov/20074534/)
15. W. Pei et al., Resolving Fates and Single-Cell Transcriptomes of Hematopoietic Stem Cell Clones by PolyloxExpress Barcoding. *Cell Stem Cell* **27**, 383–395.e8 (2020). doi: [10.1016/j.stem.2020.07.018](https://doi.org/10.1016/j.stem.2020.07.018); pmid: [32783885](https://pubmed.ncbi.nlm.nih.gov/32783885/)
16. E. E. Rosmaraki et al., Identification of committed NK cell progenitors in adult murine bone marrow. *Eur. J. Immunol.* **31**, 1900–1909 (2001). doi: [10.1002/1521-4141\(200106\)31:6<1900::AID-IMMU1900>3.0.CO;2-M](https://doi.org/10.1002/1521-4141(200106)31:6<1900::AID-IMMU1900>3.0.CO;2-M); pmid: [11433387](https://pubmed.ncbi.nlm.nih.gov/11433387/)
17. H. Nozad Charoudeh et al., Identification of an NK/T cell-restricted progenitor in adult bone marrow contributing to bone marrow- and thymic-dependent NK cells. *Blood* **116**, 183–192 (2010). doi: [10.1182/blood-2009-10-247130](https://doi.org/10.1182/blood-2009-10-247130); pmid: [20421450](https://pubmed.ncbi.nlm.nih.gov/20421450/)
18. M. L. Robinette et al., Transcriptional programs define molecular characteristics of innate lymphoid cell classes and subsets. *Nat. Immunol.* **16**, 306–317 (2015). doi: [10.1038/ni.3094](https://doi.org/10.1038/ni.3094); pmid: [25621825](https://pubmed.ncbi.nlm.nih.gov/25621825/)
19. X. Wu, Y. Chen, R. Sun, H. Wei, Z. Tian, Impairment of hepatic NK cell development in IFN- γ deficient mice. *Cytokine* **60**, 616–625 (2012). doi: [10.1016/j.cyto.2012.07.012](https://doi.org/10.1016/j.cyto.2012.07.012); pmid: [22921904](https://pubmed.ncbi.nlm.nih.gov/22921904/)
20. O. Pikovskaya et al., Cutting Edge: Eomesodermin Is Sufficient To Direct Type 1 Innate Lymphocyte Development into the Conventional NK Lineage. *J. Immunol.* **196**, 1449–1454 (2016). doi: [10.4049/jimmunol.1502396](https://doi.org/10.4049/jimmunol.1502396); pmid: [26792802](https://pubmed.ncbi.nlm.nih.gov/26792802/)
21. D. K. Sojka et al., Tissue-resident natural killer (NK) cells are cell lineages distinct from thymic and conventional splenic NK cells. *eLife* **3**, e01659 (2014). doi: [10.7554/eLife.01659](https://doi.org/10.7554/eLife.01659); pmid: [24714492](https://pubmed.ncbi.nlm.nih.gov/24714492/)
22. L. K. Mackay et al., Hobit and Blimp1 instruct a universal transcriptional program of tissue residency in lymphocytes. *Science* **352**, 459–463 (2016). doi: [10.1126/science.aad2035](https://doi.org/10.1126/science.aad2035); pmid: [27102484](https://pubmed.ncbi.nlm.nih.gov/27102484/)
23. L. M. Bradley, D. K. Dalton, M. Croft, A direct role for IFN- γ in regulation of Th1 cell development. *J. Immunol.* **157**, 1350–1358 (1996). pmid: [8759714](https://pubmed.ncbi.nlm.nih.gov/8759714/)
24. A. M. de Bruin, C. Voermans, M. A. Nolte, Impact of interferon- γ on hematopoiesis. *Blood* **124**, 2479–2486 (2014). doi: [10.1182/blood-2014-04-568451](https://doi.org/10.1182/blood-2014-04-568451); pmid: [25185711](https://pubmed.ncbi.nlm.nih.gov/25185711/)
25. L. Yang et al., IFN- γ negatively modulates self-renewal of repopulating human hematopoietic stem cells. *J. Immunol.* **174**, 752–757 (2005). doi: [10.4049/jimmunol.174.2.752](https://doi.org/10.4049/jimmunol.174.2.752); pmid: [15634895](https://pubmed.ncbi.nlm.nih.gov/15634895/)
26. A. M. de Bruin, Ö. Demirel, B. Hooibrink, C. H. Brandts, M. A. Nolte, Interferon- γ impairs proliferation of hematopoietic stem cells in mice. *Blood* **121**, 3578–3585 (2013). doi: [10.1182/blood-2012-05-432906](https://doi.org/10.1182/blood-2012-05-432906); pmid: [23487025](https://pubmed.ncbi.nlm.nih.gov/23487025/)
27. M. T. Baldrige, K. Y. King, N. C. Boles, D. C. Weksberg, M. A. Goodell, Quiescent haematopoietic stem cells are activated by IFN- γ in response to chronic infection. *Nature* **465**, 793–797 (2010). doi: [10.1038/nature09135](https://doi.org/10.1038/nature09135); pmid: [20535209](https://pubmed.ncbi.nlm.nih.gov/20535209/)
28. F. Ginhoux, M. Guilliams, Tissue-Resident Macrophage Ontogeny and Homeostasis. *Immunity* **44**, 439–449 (2016). doi: [10.1016/j.immuni.2016.02.024](https://doi.org/10.1016/j.immuni.2016.02.024); pmid: [26982352](https://pubmed.ncbi.nlm.nih.gov/26982352/)
29. E. G. Perdiguer, F. Geissmann, The development and maintenance of resident macrophages. *Nat. Immunol.* **17**, 2–8 (2016). doi: [10.1038/ni.3341](https://doi.org/10.1038/ni.3341); pmid: [26681456](https://pubmed.ncbi.nlm.nih.gov/26681456/)
30. P. Zeis et al., In Situ Maturation and Tissue Adaptation of Type 2 Innate Lymphoid Cell Progenitors. *Immunity* **53**, 775–792.e9 (2020). doi: [10.1016/j.immuni.2020.09.002](https://doi.org/10.1016/j.immuni.2020.09.002); pmid: [33002412](https://pubmed.ncbi.nlm.nih.gov/33002412/)
31. S. Koga et al., Peripheral PDGFR α ⁺gp38⁺ mesenchymal cells support the differentiation of fetal liver-derived LIC2. *J. Exp. Med.* **215**, 1609–1626 (2018). doi: [10.1084/jem.20172310](https://doi.org/10.1084/jem.20172310); pmid: [29728440](https://pubmed.ncbi.nlm.nih.gov/29728440/)
32. E. Narni-Mancinelli et al., Fate mapping analysis of lymphoid cells expressing the Nkp46 cell surface receptor. *Proc. Natl. Acad. Sci. U.S.A.* **108**, 18324–18329 (2011). doi: [10.1073/pnas.1112064108](https://doi.org/10.1073/pnas.1112064108); pmid: [22021440](https://pubmed.ncbi.nlm.nih.gov/22021440/)
33. S. B. Su et al., Altered chemokine profile associated with exacerbated autoimmune pathology under conditions of genetic interferon- γ deficiency. *Invest. Ophthalmol. Vis. Sci.* **48**, 4616–4625 (2007). doi: [10.1167/iov.07-0233](https://doi.org/10.1167/iov.07-0233); pmid: [17898285](https://pubmed.ncbi.nlm.nih.gov/17898285/)
34. W. Hsu et al., Differential mechanisms in the pathogenesis of autoimmune cholangitis versus inflammatory bowel disease in interleukin-2R α ^{-/-} mice. *Hepatology* **49**, 133–140 (2009). doi: [10.1002/hep.22591](https://doi.org/10.1002/hep.22591); pmid: [19065673](https://pubmed.ncbi.nlm.nih.gov/19065673/)
35. Y. Moritoki et al., B cells suppress the inflammatory response in a mouse model of primary biliary cirrhosis. *Gastroenterology* **136**, 1037–1047 (2009). doi: [10.1053/j.gastro.2008.11.035](https://doi.org/10.1053/j.gastro.2008.11.035); pmid: [19118554](https://pubmed.ncbi.nlm.nih.gov/19118554/)
36. J. Wang et al., Poly I:C prevents T cell-mediated hepatitis via an NK-dependent mechanism. *J. Hepatol.* **44**, 446–454 (2006). doi: [10.1016/j.jhep.2005.08.015](https://doi.org/10.1016/j.jhep.2005.08.015); pmid: [16310275](https://pubmed.ncbi.nlm.nih.gov/16310275/)
37. E. Esplugues et al., Control of Th17 cells occurs in the small intestine. *Nature* **475**, 514–518 (2011). doi: [10.1038/nature10228](https://doi.org/10.1038/nature10228); pmid: [21765430](https://pubmed.ncbi.nlm.nih.gov/21765430/)
38. J. Wang et al., Respiratory influenza virus infection induces intestinal immune injury via microbiota-mediated Th17 cell-dependent inflammation. *J. Exp. Med.* **211**, 2397–2410 (2014). doi: [10.1084/jem.20140625](https://doi.org/10.1084/jem.20140625); pmid: [25366965](https://pubmed.ncbi.nlm.nih.gov/25366965/)
39. J. P. Marcove et al., TGF- β is responsible for NK cell immaturity during ontogeny and increased susceptibility to infection during mouse infancy. *Nat. Immunol.* **13**, 843–850 (2012). doi: [10.1038/ni.2388](https://doi.org/10.1038/ni.2388); pmid: [22863752](https://pubmed.ncbi.nlm.nih.gov/22863752/)
40. N. S. Williams et al., Differentiation of NK1.1⁺, Ly49⁺ NK cells from flt3⁺ multipotent marrow progenitor cells. *J. Immunol.* **163**, 2648–2656 (1999). pmid: [10453005](https://pubmed.ncbi.nlm.nih.gov/10453005/)
41. R. Satija, J. A. Farrell, D. Gennert, A. F. Schier, A. Regev, Spatial reconstruction of single-cell gene expression data. *Nat. Biotechnol.* **33**, 495–502 (2015). doi: [10.1038/nbt.3192](https://doi.org/10.1038/nbt.3192); pmid: [25867923](https://pubmed.ncbi.nlm.nih.gov/25867923/)

ACKNOWLEDGMENTS

We thank S. Su for the GKO mice and A. Tedgui for the *Irfn^{fl/fl}* mice. **Funding:** We acknowledge funding support from the following sources: Natural Science Foundation of China (81788101, 92042305, 81922029, and 8176112803), National Key R&D Program of China (2019YFA0508502/3 and 2020YFA0804100), and Chinese Academy of Medical Sciences (CAMS) Innovation Fund for Medical Sciences (CIFMS 2019-I2M-5-073). The E.V. laboratory at CIML and Assistance-Publique des Hôpitaux de Marseille is supported by funding from the European Research Council (ERC) under the European Union's Horizon 2020 research and innovation program (TILC, grant agreement 694502 and Minfla-TILC, grant agreement 875102 - Minfla-Tilc), the Agence Nationale de la Recherche including the PIONEER Project (ANR-17-RHUS-0007), MSDAvenir, Innate Pharma and institutional grants to the CIML (INSERM, CNRS, and Aix-Marseille University) and to Marseille Immunology. **Author contributions:** L.B., Y.K., L.T., R.S., E.V., H.P., and Z.T. initiated and designed the research. L.B., L.T., H.P., E.V., and Z.T. wrote the manuscript. L.B., M.V., Y.K., M.E., B.E., J.G., L.T., and H.P. performed all experiments and analyzed and interpreted the results. H.W. contributed to the discussion of the results. **Competing interests:** E.V. is an employee of Innate Pharma. None of the other authors have any competing interests to declare. **Data and materials availability:** All data are available in the main text or the supplementary materials. All sequencing data have been deposited at the NCBI Gene Expression Omnibus depository and are accessible with the accession number GSE165785.

SUPPLEMENTARY MATERIALS

[science.sciencemag.org/content/\[vol\]/\[issue\]/eaba4177/suppl/DC1](https://science.sciencemag.org/content/[vol]/[issue]/eaba4177/suppl/DC1)
Figs. S1 to S10
Tables S1 and S2
MDAR Reproducibility Checklist

[View/request a protocol for this paper from Bio-protocol.](#)

4 December 2019; resubmitted 10 May 2020
Accepted 2 February 2021
10.1126/science.aba4177